Journal of the Korean Astronomical Society
50: 41 ∼ 49, 2017 June

https://doi.org/10.5303/JKAS.2017.50.3.41
pISSN: 1225-4614 · eISSN: 2288-890X
http://jkas.kas.org

Photometric Study of NPA Rotator (5247) Krylov

Hee-Jae Lee[1,2], Hong-Kyu Moon[2], Myung-Jin Kim[2], Chun-Hwey Kim[1], Josef Ďurech[3], Young-Jun Choi[2,4], Young-Seok Oh[2,5], Jintae Park[2], Dong-Goo Roh[2], Hong-Suh Yim[2], Sang-Mok Cha[2,5], and Yongseok Lee[2,5]

[1]Department of Astronomy and Space Science, Chungbuk National University, 1 Chungdae-ro, Seowon-gu, Cheongju, Chungbuk 28644, Korea; hjlee@kasi.re.kr, kimch@chungbuk.ac.kr
[2]Korea Astronomy and Space Science Institute, 776 Daedeokdae-ro, Yuseong-gu, Daejeon 34055, Korea; fullmoon, skarma, yjchoi, yso1987, jtpark, rrdong9, yimhs, chasm, yslee@kasi.re.kr
[3]Institute of Astronomy, Faculty of Mathematics and Physics, Charles University, Prague, V Holesovickach 2, CZ-18000 Prague 8, Czech Republic; durech@sirrah.troja.mff.cuni.cz
[4]Astronomy and Space Science, University of Science and Technology, 217 Gajeong-ro, Yuseong-gu, Daejeon 34113, Korea
[5]School of Space Research, Kyung Hee University, 1732 Deogyeong-daero, Giheung-gu, Yongin, Gyeonggi 17104, Korea

Received March 31, 2017; accepted May 8, 2017

Abstract: We conduct BVRI and R band photometric observations of asteroid (5247) Krylov from January 2016 to April 2016 for 51 nights using the Korea Microlensing Telescope Network (KMTNet). The color indices of (5247) Krylov at the light curve maxima are determined as $B-V = 0.841 \pm 0.035$, $V-R = 0.418 \pm 0.031$, and $V-I = 0.871 \pm 0.031$ where the phase angle is 14.1°. They are acquired after the standardization of BVRI instrumental measurements using the ensemble normalization technique. Based on the color indices, (5247) Krylov is classified as a S-type asteroid. Double periods, that is, a primary period $P_1 = 82.188 \pm 0.013$ h and a secondary period $P_2 = 67.13 \pm 0.20$ h are identified from period searches of its R band light curve. The light curve phases with P_1 and this indicate that it is a typical Non-Principal Axis (NPA) asteroid. We discuss the possible causes of its NPA rotation.

Key words: minor planets, asteroids: individual: (5247) Krylov — minor planets, asteroids: non-principal axis rotation — telescopes: KMTNet — technique: photometric

1. Introduction

The spin state of an asteroid is considered a vital clue to study either its physical properties or spin evolution history. It is classified into two different states according to the Euler angle between the orientation of the principal axis and the rotational angular momentum vector. When the angular momentum vector is aligned with a principal axis, it is called Principal Axis (PA) rotation, thus the asteroid performs a constant axial rotation. In contrast, when the angular momentum vector is misaligned, it is called NPA rotation. Then the asteroid develops into a dynamically unstable state so that the spin axis shows excited precession around the angular momentum vector. Hence, rotation and precession periods occur simultaneously in the light curve. The NPA rotation was termed "tumbling" by Harris (1994) and has been generally used since then.

Most studies on asteroid light curves have long been focused on PA rotation. The number of observed samples of NPA rotators including NPA candidates as of April 2017 is about 80 (Warner et al. 2009). Even if such an object was observed, it was difficult for the NPA rotation to be unambiguously detected. This is why studies on NPA rotation have been very limited. However, with recent development of observational techniques, photometric precision has improved so that previously undetected anomalies can be found and properly investigated. At the same time, the number of asteroid light curves has increased, thanks to the growth in the number of available telescopes and improvements in observational efficiency, leading to an increase in the inventory of NPA rotators. Further, we can not only determine their angular momentum vectors within a relatively short period of time, but also investigate their physical properties as we are able to see their facets over a wide range of regions on their surfaces based on observations during several apparitions. Thanks to a proper understanding of precession, the scientific significance of NPA rotators has only been grasped recently, and we can now reconstruct the tumbling motions of asteroids from the analysis of light curve.

The first known NPA rotator was (4179) Toutatis, which was discovered by radar observation by Hudson & Ostro (1995). Kaasalainen (2001) proposed an inversion method for the first time using photometry data in which a numerical model is applied to the light curve of an asteroid that exhibits NPA rotation. Pravec et al. (2005) carried out period and orientation analyses assuming the shapes of four asteroids, (4179) Toutatis, (54789) 2001 MZ7, 2000 WL107 and 2002 TD60, to be approximately a tri-axial ellipsoid using the inversion method. There have only been two NPA rotators for which precise physical models were constructed using the light curve inversion method previously mentioned: 2008 TC3 (Scheirich et al. 2010) and (99942) Apophis

Corresponding author: H.-J. Lee

Table 1
Observation log

Date UT	R.A. (h m)	Dec. (° ′)	d (AU)	r (AU)	α (°)	Site	Filter	Weather[1]
2016-01-27	08 44	–20 26	1.650	2.492	14.5	SAAO	R	3
2016-01-28	08 43	–20 26	1.646	2.490	14.4	SAAO	R	1
2016-01-29	08 42	–20 25	1.642	2.489	14.3	SSO	R	1
2016-01-29	08 42	–20 25	1.642	2.489	14.3	SAAO	R	0
2016-02-03	08 37	–20 15	1.626	2.481	14.0	SSO	R	3
2016-02-04	08 36	–20 12	1.624	2.479	14.0	SAAO	BVRI	1
2016-02-05	08 35	–20 08	1.621	2.478	14.0	SAAO	BVRI	0
2016-02-06	08 34	–20 04	1.619	2.476	14.0	SAAO	BVRI	0
2016-02-07	08 33	–20 00	1.618	2.474	14.0	SSO	BVRI	0
2016-02-07	08 33	–20 00	1.617	2.474	14.0	SAAO	BVRI	4
2016-02-08	08 32	–19 55	1.616	2.473	14.0	SSO	BVRI	1
2016-02-08	08 32	–19 55	1.616	2.473	14.0	SAAO	BVRI	3
2016-02-09	08 31	–19 50	1.615	2.471	14.1	SSO	BVRI	0
2016-02-10	08 30	–19 45	1.613	2.470	14.1	SSO	BVRI	0
2016-02-10	08 30	–19 45	1.613	2.470	14.1	SAAO	BVRI	0
2016-02-20	08 20	–18 30	1.614	2.453	15.1	SSO	R	1
2016-02-22	08 19	–18 16	1.616	2.451	15.3	CTIO	R	0
2016-02-22	08 19	–18 12	1.615	2.451	15.2	SSO	R	1
2016-02-22	08 18	–18 09	1.617	2.449	15.4	SAAO	R	0
2016-02-24	08 18	–17 57	1.619	2.447	15.6	CTIO	R	0
2016-02-24	08 17	–17 52	1.620	2.446	15.7	SSO	R	0
2016-02-24	08 17	–17 49	1.621	2.446	15.8	SAAO	R	1
2016-02-28	08 15	–17 16	1.629	2.441	16.3	CTIO	R	0
2016-02-28	08 15	–17 11	1.630	2.440	16.4	SSO	R	1
2016-02-28	08 14	–17 07	1.631	2.439	16.5	SAAO	R	0
2016-02-30	08 14	–16 54	1.634	2.437	16.7	CTIO	R	0
2016-03-01	08 13	–16 50	1.636	2.436	16.8	SSO	R	0
2016-03-01	08 13	–16 45	1.637	2.436	16.9	SAAO	R	0
2016-03-03	08 13	–16 32	1.641	2.434	17.1	CTIO	R	0
2016-03-03	08 12	–16 27	1.642	2.433	17.2	SSO	R	0
2016-03-03	08 12	–16 11	1.648	2.431	17.5	SAAO	R	0
2016-03-05	08 12	–16 09	1.648	2.430	17.5	CTIO	R	0
2016-03-05	08 12	–16 04	1.650	2.430	17.6	SSO	R	0
2016-03-07	08 11	–15 45	1.656	2.427	17.9	CTIO	R	3
2016-03-07	08 11	–15 36	1.660	2.426	18.1	SAAO	R	4
2016-03-11	08 10	–14 57	1.674	2.420	18.8	CTIO	R	0
2016-03-15	08 09	–14 07	1.695	2.413	19.6	CTIO	R	0
2016-03-15	08 09	–13 57	1.700	2.412	19.7	SAAO	R	3
2016-03-22	08 09	–12 35	1.740	2.400	21.0	SSO	R	0
2016-03-24	08 09	–12 15	1.750	2.397	21.3	CTIO	R	0
2016-03-24	08 09	–12 10	1.753	2.397	21.3	SSO	R	1
2016-03-24	08 09	–12 05	1.756	2.396	21.4	SAAO	R	4
2016-03-26	08 09	–11 51	1.764	2.394	21.7	CTIO	R	1
2016-03-26	08 09	–11 46	1.766	2.393	21.8	SSO	R	1
2016-03-28	08 10	–11 26	1.778	2.390	22.0	CTIO	R	0
2016-03-30	08 10	–11 02	1.792	2.387	22.4	CTIO	R	0
2016-03-30	08 10	–10 58	1.795	2.386	22.4	SSO	R	0
2016-04-03	08 12	–10 06	1.829	2.378	23.1	SAAO	R	0
2016-04-05	08 13	–09 48	1.841	2.375	23.3	SSO	R	0
2016-04-10	08 16	–08 58	1.879	2.367	23.9	CTIO	R	0
2016-04-10	08 16	–08 49	1.885	2.366	24.0	SAAO	R	0

[1] Night-averaged weather condition codes: clear (0), partly cloudy (1), strong wind (2) and higher humidity (4). (Code 3: "unclear".)

(Pravec et al. 2014), both of which are Near Earth Asteroids (NEAs). Until recently, studies on NPA rotators have been focused only on NEAs and no investigations have been conducted for MBAs (Main Belt Asteroids). However since the Main Belt (MB) is dynamically stable except for resonance regions that are affected significantly either by major planets or Yarkovsky drift, the orbits of asteroids have not changed significantly since formation. Because of this, the MBAs play a crucial role in studying the orbit and spin evolution of asteroids caused by non-gravitational forces or collisions. We selected MBAs known to be NPA rotator candidates in

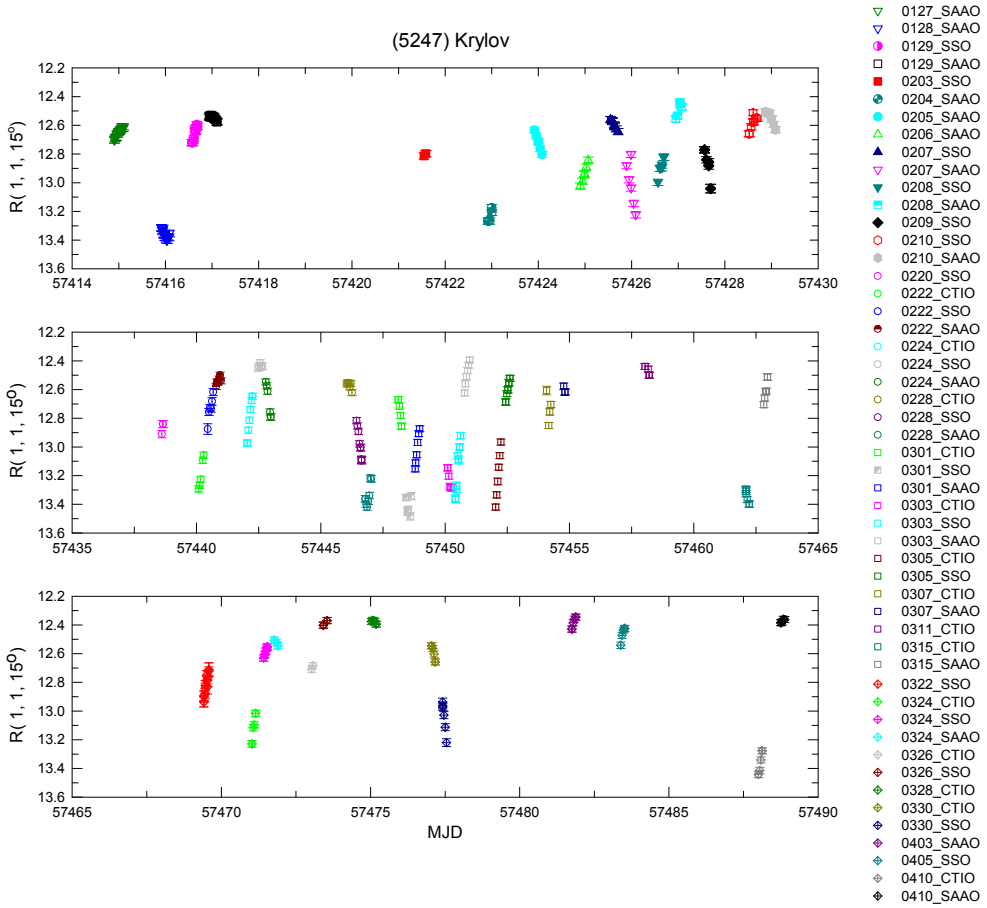

Figure 1. Geo- and heliocentric distance and solar phase angle-corrected R-band light curve of (5247) Krylov.

the asteroid Light Curve Data Base (LCDB; Warner et al. 2009) and performed a series of time-series observations to verify if the selected objects clearly show NPA rotation. The present study reports our photometric study on the MB asteroid (5247) Krylov.

(5247) Krylov was discovered by Karachkina (1982) (Marsden & Williams 1993). It belongs to the Phocaea asteroid family in the inner MB and the established orbital elements are $a = 2.33$ AU, $e = 0.208$, and $\sin i = 0.40$. Time-series photometry of this asteroid was conducted by Donald Pray and Adrian Galad for the first time (Pravec, personal communication, 2016), and Pravec et al. (2006)[1] employed time-series photometry to detect the double period ($P_1 = 81.5$ h, $P_2 = 68.5$ h) and classified it as a NPA rotator candidate. On the other hand, Gil-Hutton (2006) proposed the presence of the Krylov group inside the Phocaea family based on his Hierarchical Clustering Method (HCM) runs – thereby suggesting that (5247) Krylov shows evidence of collision after the formation of the Phocaea family.

In order to check if (5247) Krylov really exhibits an unstable state of rotation, BVRI and R band time-series photometry were conducted using KMTNet over an extended period of time and higher temporal resolution. In Section 2, observations of (5247) Krylov and data reduction method are described. In Section 3, taxonomic classification of the asteroid from the BVRI multiband observation is explained. In Section 4, the period analysis of R-band light curves and the analysis results are presented. Finally, in Section 5, we summarize the results and discuss the most likely causes of the current spin state of (5247) Krylov.

2. OBSERVATIONS AND DATA REDUCTION

We conducted photometric observations of (5247) Krylov at the three sites of KMTNet (Kim et al. 2016): the Cerro-Tololo Inter-American Observatory (CTIO) in Chile, the South African Astronomical Observatory (SAAO) in South Africa, and the Siding Spring Observatory (SSO) in Australia. KMTNet consists of 1.6-m wide-field optical telescopes and 18K × 18K mosaicked CCDs with four 9K × 9K e2v chips. The pixel scale of the CCD camera is 0.4″/pixel and the resulting field of view is four square degrees. KMTNet sites are well separated in geographic longitude, thus enabling continuous observations during the runs when telescope times are allocated at all three sites. The wide-field of view and round-the clock operation capabilities of KMTNet allows discovery, astrometry and follow-up

[1] http://www.asu.cas.cz/~ppravec/newres.txt

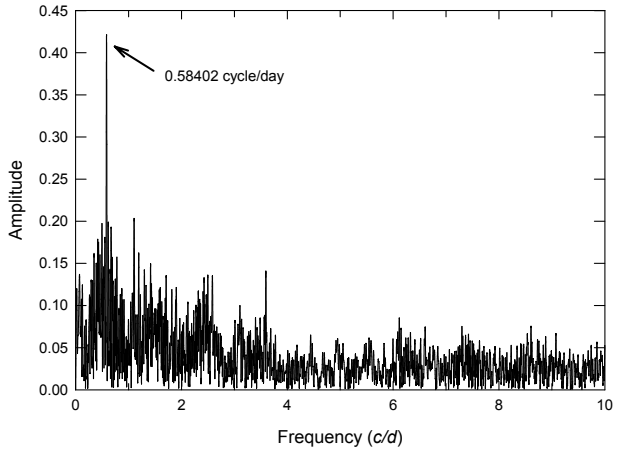

Figure 2. Amplitude spectra of P_1 using `Period04`

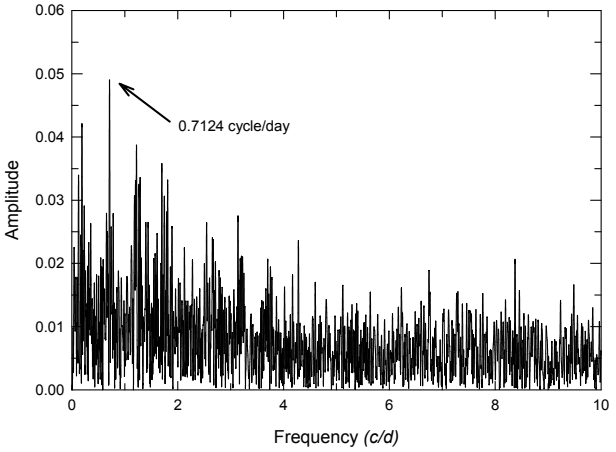

Figure 3. Amplitude spectra of P_2 using `Period04`

physical characterization of asteroids in a most efficient manner. We call the dedicated software subsystem, the computing facility, research activities, members and partner organizations the Deep Ecliptic Patrol of the Southern Sky (DEEP-South; Moon et al. 2015). We employed the target of opportunity observations (TO) of the DEEP-South for this study. In the present paper, time-series photometry was conducted using Johnson-Cousins R-filter to obtain the light curve of (5247) Krylov. Simultaneously, multi-band photometry utilizing Johnson-Cousins BVRI filters was also carried out to determine its taxonomy. R-band time-series observations were carried out for a total of 51 nights from January to April 2016, and BVRI multi-band photometry was conducted in February 2016 for a total of 10 nights. Since the primary period disclosed by Pravec (2006) was 81.5 hours, the observation cadence was 1 h on average and exposure time was selected from 15 sec to 30 sec during the runs considering the signal-to-noise ratio (SNR) and its projected motion in the sky

The equatorial coordinates, geo- and heliocentric distances and solar phase angle of (5247) Krylov at the time of observation are presented in Table 1. Preprocessing of raw observed images was completed using the KMTNet pre-processing software (Kim et al. 2016), hence crosstalk, overscan, bias and flat fielding corrections and trimming were applied. The world coordinate system (WCS) solution of the observed images is calculated using the USNO B1.0 catalog and matched with SCAMP (Bertin 2005) with an average astrometric error of $1.5''$. Post-processing is carried out using the Asteroid Spin Analysis Package (ASAP) (Kim 2014), which applies aperture photometry utilizing the IRAF/APPHOT package.

The standardization employed in the present study is an ensemble normalization technique (Gilliland et al. 1988; Kim et al. 1999) making use of the American Association of Variable Star Observers Photometric All-Sky Survey (APASS) catalog (Munari et al. 2014). The SDSS magnitudes in the APASS catalog are fitted with the Johnson-Cousins photometric system based on transformation equations proposed by Jordi et al. (2006). The calibrated magnitude error is $R \sim 0.02$ to 0.05 taking into account the instrumental magnitude and the zero magnitude error.

3. RESULTS

3.1. Spin State

The tumbling motion of any asteroid exhibits a complex light curve of double periods. This happens because rotation and precession of a tumbling body occur at the same time. According to Kaasalainen (2001), these double periods are linear combinations of rotation period (P_ψ) and precession period (P_ϕ). In order to confirm the tumbling motion of (5247) Krylov, period analysis on the observed light curve was conducted. Prior to performing the analysis, the magnitude variation due to changes in geo- and heliocentric distances and solar phase angle was corrected in order to examine only the light variation generated due to the changes in the viewing cross section caused by rotation and precession. The magnitude variation-corrected reduced magnitude caused by changes in geo- and heliocentric distance is corrected to a position where geo- and heliocentric is 1 AU using the method proposed by Buchheim (2010), and the light travel time (LTT) effect is corrected using

$$T_{LT} = T_{obs} - \Delta/c \quad (1)$$

where T_{LT} refers to LTT-corrected time at the asteroid, T_{obs} to the observed time, Δ to the geocentric distance, and c to the speed of light. In addition, the solar phase angle is corrected to 15 degree using the H-G model proposed by Bowell et al. (1989). For geo- and heliocentric distances and solar phase angle, ephemeris provided by JPL Horizon is used and $G = 0.15$ which is an average value of the vast majority of asteroids (Vereš et al. 2015). The final corrected light curve is presented in Figure 1. As is shown, different data points are distinguished by various symbols according to the observation sites and the dates when our observations were made.

`Period04` (Lenz & Breger 2005) is used to find periodicities in the light curve, as shown in Figure 1.

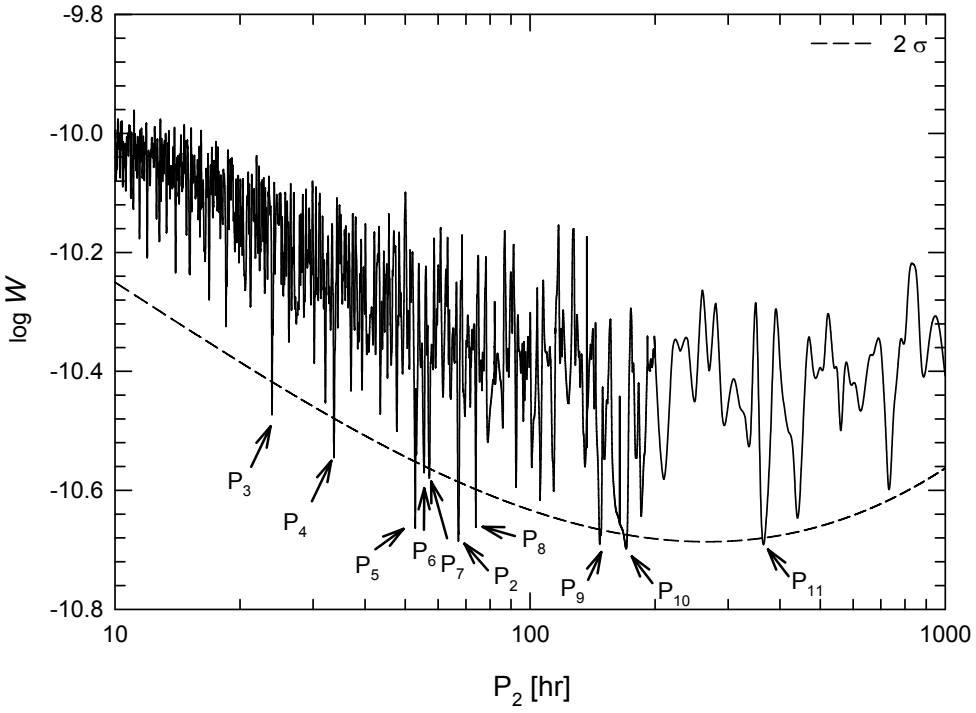

Figure 4. W vs. P_2 for the 3rd order 2-dimensional Fourier series with $P_1 = 82.2$ h (solid line) and the 2σ range of W (dotted line).

Table 2
Harmonics of the P_2 candidate

	Period (h)	Harmonics
P_3	23.88	$1/P_3 = 1/P_1 + 2/P_2$
P_4	33.66	$1/P_4 = 2/P_2$
P_5	52.85	$1/P_5 = 4/P_1 - 2/P_2$
P_6	55.50	$3/P_6 = 2/P_1 + 2/P_2$
P_7	57.14	$1/P_7 = -1/P_1 + 2/P_2$
P_8	73.95	$2/P_8 = 1/P_1 + 1/P_2$
P_9	147.21	$2/P_9 = 1/P_8$
P_{10}	170.37	$3/P_{10} = 1/P_7$
P_{11}	366.07	$1/P_{11} = -1/P_1 + 1/P_2$

`Period04` is a period analysis program based on discrete Fourier transform and multiple-least-squares algorithms (Sperl 1998). Figure 2 shows the power spectrum generated with `Period04`, in which the frequency of the largest amplitude is unambiguously shown at 0.58402 cycles/day. This frequency occurs when the light curve has a single peak. However, asteroids are considered to have even albedo over the surface and a shape that can be approximated to a tri-axial ellipsoid, hence the reflected light varies due to rotation, and precession when NPA rotation takes place at the same time, so that the light curve reveals double peaks. Accordingly, we determine the corresponding period $P_1 = 1/f_1 = 82.188 \pm 0.013$ h based on half of the frequency $f_1 = 0.29201$ cycles/day.

We determined the secondary period (P_2) using `Period04` to remove the light variation caused by P_1 from the light curve. Figure 3 shows the power spectrum of the residuals. The frequency at the highest amplitude is 0.7124 cycles/day and half of the frequency, 0.3562 cycles/day, is set to f_2 that corresponds to the double peak light curve. The corresponding $P_2 = 1/f_2$ is 67.37 h ($\pm$ 0.15 h). However the P_2 has a signal rather weaker than P_1. Hence, we tried another method and used the 2-dimensional Fourier series as proposed by Pravec et al. (2005) for confirmation:

$$\begin{aligned}\mathbf{F}\left(\psi\left(\mathbf{t}\right),\phi\left(\mathbf{t}\right)\right) = {} & C_0 \\ & + \sum_{j=1}^{m}\left[C_{j0}\cos\frac{2\pi j}{P_a}t + S_{j0}\sin\frac{2\pi j}{P_a}t\right] \\ & + \sum_{k=1}^{m}\sum_{j=-m}^{m}\left[C_{jk}\cos\left(\frac{2\pi j}{P_a}+\frac{2\pi j}{P_b}\right)t\right. \\ & \left. + S_{jk}\sin\left(\frac{2\pi j}{P_a}+\frac{2\pi j}{P_b}\right)t\right] \qquad (2)\end{aligned}$$

Here, P_a refers to the period whose amplitude is larger than P_b. The time-series light curve presented in Figure 1 is fitted to Equation (2). The order of the Fourier series used here is $m = 3$. The reason for adopting $m = 3$ is as follows. If a higher order is used, more complicated features can be fitted but they might be confused with periods which are fitted by higher order terms. Once the observed values are fitted to Equation (2), P_a is fixed to P_1 (82.188 h) found with `Period04`, and then P_2 is increased from 10 h to 1000 h with 0.01 h step size increments and then we can determine the harmonics coefficients in Equation (2) by matching

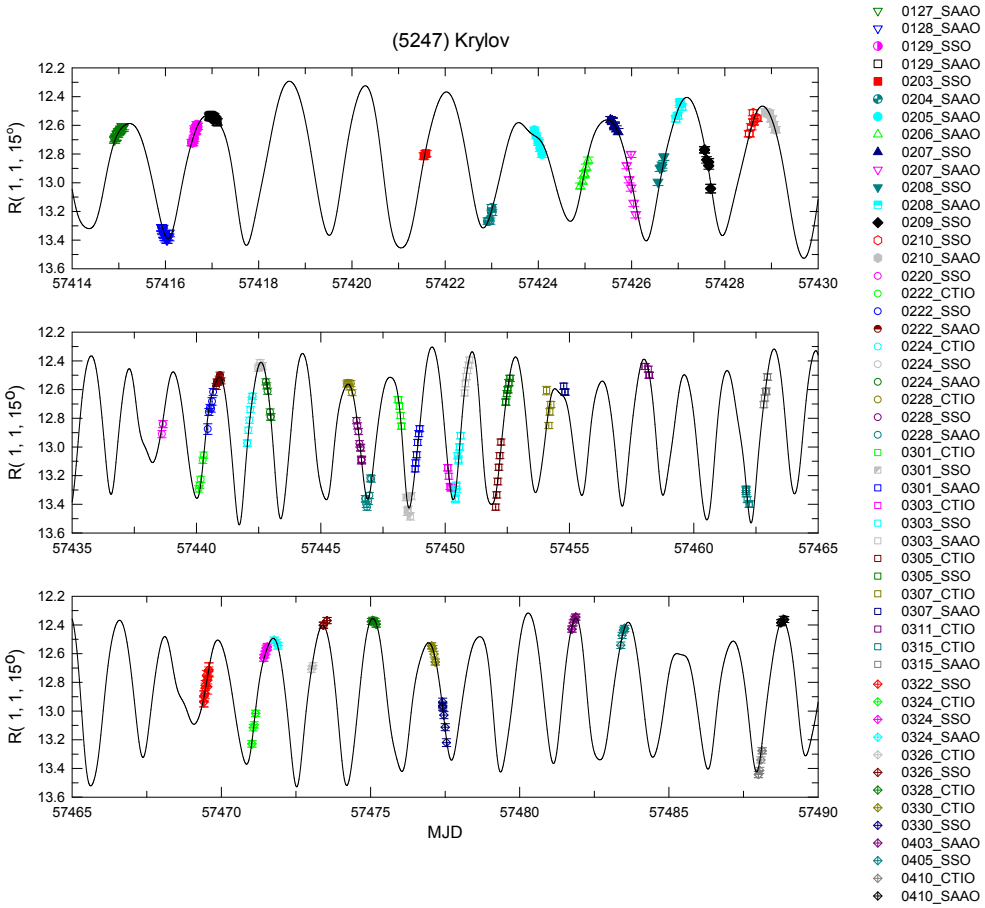

Figure 5. The 2-dimensional Fourier series (solid line) with $P_1 = 82.188$ h and $P_2 = 67.13$ h, plotted over Figure 1.

Table 3
Coefficients of the 3rd-order 2-dimensional Fourier series

Coefficient	Value	Coefficient	Value	Coefficient	Value
C_0	0.643	$C_{2,1}$	0.0101	$S_{3,2}$	-0.0046
$C_{1,0}$	-0.0127	$S_{2,1}$	0.0001	$C_{-3,1}$	-0.0008
$S_{1,0}$	-0.0035	$C_{3,1}$	0.0044	$S_{-3,1}$	0.0203
$C_{2,0}$	0.0375	$S_{3,1}$	0.0037	$C_{-2,1}$	-0.0283
$S_{2,0}$	-0.2571	$C_{-3,2}$	-0.0093	$S_{-2,1}$	-0.003
$C_{3,0}$	-0.0103	$S_{-3,2}$	0.0061	$C_{-1,1}$	-0.0019
$S_{3,0}$	0.006	$C_{-2,2}$	0.0169	$S_{-1,1}$	0.0017
$C_{-3,1}$	-0.0185	$S_{-2,2}$	0.0073	$C_{0,1}$	-0.0057
$S_{-3,1}$	0.0056	$C_{-1,2}$	0.0005	$S_{0,1}$	0.0068
$C_{-2,1}$	0.0128	$S_{-1,2}$	-0.0005	$C_{1,1}$	0.0044
$S_{-2,1}$	0.0076	$C_{0,2}$	0.0307	$S_{1,1}$	0.0016
$C_{-1,1}$	-0.0198	$S_{0,2}$	-0.0321	$C_{2,1}$	-0.0019
$S_{-1,1}$	-0.0051	$C_{1,2}$	0.0047	$S_{2,1}$	0.0053
$C_{0,1}$	0.028	$S_{1,2}$	-0.0163	$C_{3,1}$	-0.0032
$S_{0,1}$	0.0084	$C_{2,2}$	0.0042	$S_{3,1}$	0.0045
$C_{1,1}$	-0.003	$S_{2,2}$	-0.0118		
$S_{1,1}$	0.0242	$C_{3,2}$	0.0012		

the observed light curve with Equation (2), and calculate the sum of squared residuals ($W{=}\Sigma(O-C)^2$) of differences between the observed and modeled light curves. Figure 4 shows W expressed as a function of P_b. $P_b = 67.13 \pm 0.20$ h, which shows the highest signal to noise ratio in Figure 4 matched with $P_2 = 67.37 \pm 0.15$ h acquired using `Period04` within a range of error. Frequencies of the peaks whose W is 2σ or higher in Figure 4 are presented in Table 2. They were studied in detail and it was found that all frequencies can be represented

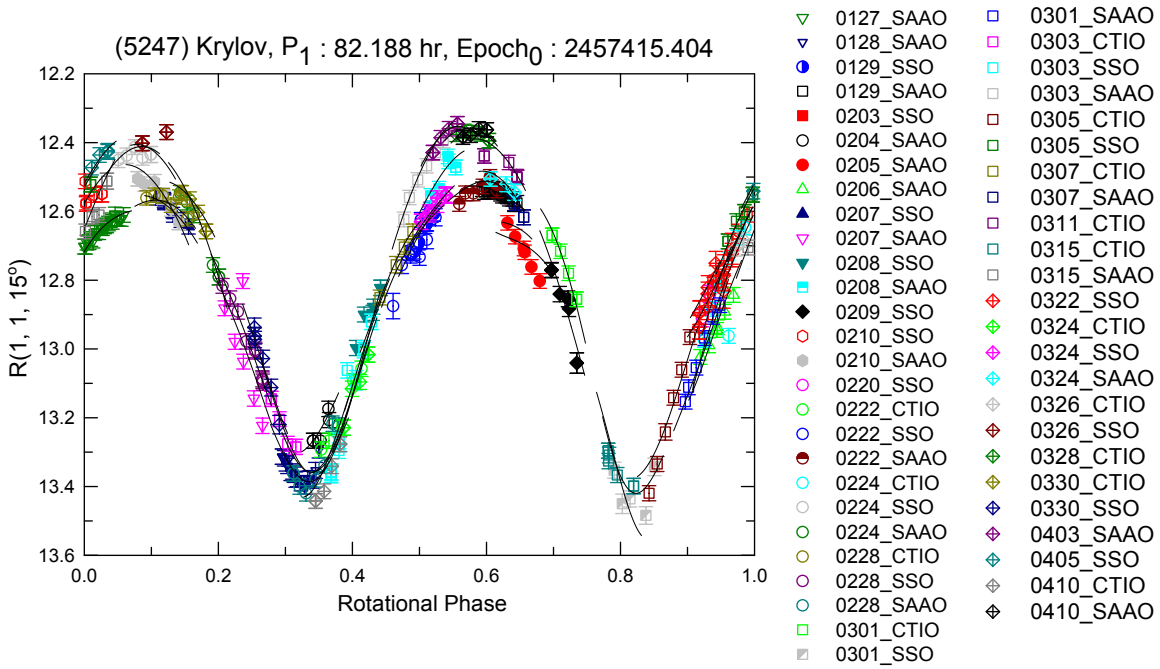

Figure 6. Same as Figure 5 but in the phase domain, using the period $P_1 = 82.188$ h.

Table 4
Double periods of (5247) Krylov

	Periods	
P_1 [h]	82.188 ± 0.013	
P_2 [h]	$67.37^{1} \pm 0.15$	$67.13^{2} \pm 0.20$

[1] Obtained from `Period04`.
[2] Obtained from 2-dimensional Fourier analysis.

Table 5
Color Indices of (5247) Krylov

	Color Indices
$B-V$	0.841 ± 0.037
$V-R$	0.418 ± 0.031
$V-I$	0.871 ± 0.031

by a combination of P_a and P_b. Table 3 shows the coefficients of the Fourier series in Equation (2) determined in the current work. Figure 5 displays the time-series light curves with coefficients listed in Table 3 and Equation (2), while Figure 6 shows light curve phased with P_1. The light curve in Figure 6 shows significant deviations rather than a perfect folding at each phase, revealing the typical light curve of a NPA rotator.

The model light curve generated with the 2-dimensional Fourier series in Equation (2) most closely reconstructs the observations using P_1 and P_2 obtained in the present study. The P_1 and P_2 values are shown in Table 4. As depicted in Figures 5 and 6, the double period feature in this modeled light variation confirms that (5247) Krylov is a NPA asteroid.

3.2. Taxonomy

The taxonomy is determined using the color indices obtained from standardization of BVRI multi-band photometry. With the color indices acquired from the photometry, the closest values to the light curve maxima are selected and used. The light curve maxima implies that the widest cross section of the asteroid can be seen by an observer at the time of observation. Therefore, since the color indices at the light curve maxima best represent its overall surface property, they were adopted as shown in Table 5. Based on the values, taxonomy of this object is found to be S-type using the classification method proposed by Dandy et al. (2003) as depicted in Figures 7 and 8. This is the same as the representative taxonomy of the Phocaea family, the parent family of (5247) Krylov (Carruba 2009). In addition, the albedo of this asteroid is 0.171 ± 0.013 (Usui et al. 2011) which is consistent with S-type (0.216 ± 0.086; Usui et al. 2011).

4. SUMMARY AND DISCUSSIONS

In this study, we carried out BVRI and R band photometric observations of asteroid (5247) Krylov for a total of 51 nights using KMTNet. The asteroid is categorized as S-type based on the diagram drawn by Dandy et al. (2003) and using the color indices obtained from our BVRI photometry. We acquired the light curve where only a change in the viewing cross section due to rotation and precession is found in the R band. The period analysis reveals a long double period with $P_1 = 82.188$ h and $P_2 = 67.13$ h. With these periods, we reconstruct the full-coverage light curve of (5247) Krylov and confirm that it is a NPA rotator in the MB.

According to Pravec et al. (2014), the plausible

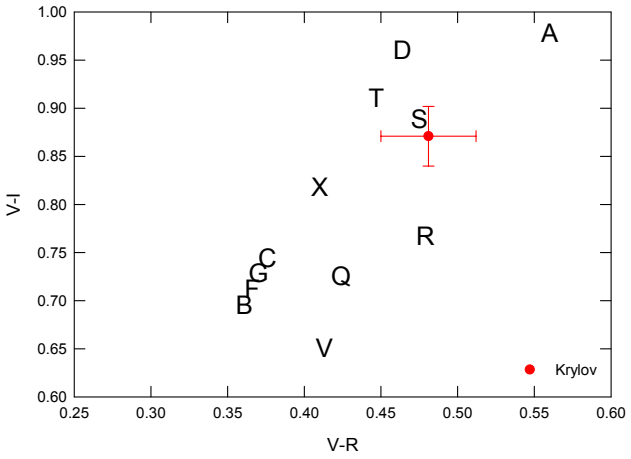

Figure 7. The $V-R$ vs. $V-I$ two-color diagram of different taxonomic types. The assorted characters represent different taxonomic types according to Dandy et al. (2003). The red dot represents (5247) Krylov.

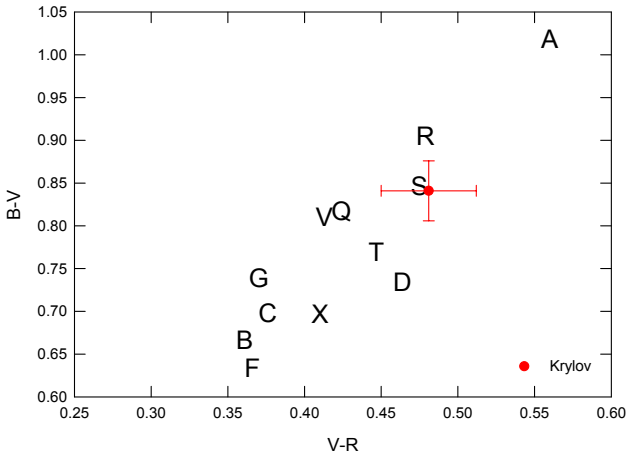

Figure 8. The $V-R$ vs. $B-V$ two-color diagram of different taxonomic types. Characters and red dot are the same as in Figure 7.

causes of NPA rotation of an asteroid can be attributed to the following four cases: (1) Catastrophic disruption(s) of a parent body, thereby creating a kilometer-sized smaller asteroid. (2) A sub-catastrophic impact. (3) Spin-down due to the YORP effect. (4) Gravitational pull during a planetary flyby. Based on the above-mentioned possibilities, we can speculate on the formation scenario of (524) Kryolv. According to Farinella et al. (1998), the collisional life-time of a MBA is $\tau_{\rm collision} = KD_m^{0.5}$ with $K \simeq 400$ Myr where D_m is the diameter in units of kilometers. If we apply 10.44 ± 0.37 km, the diameter of (5247) Krylov given in the AcuA, we have $\tau_{\rm collision} \simeq 1.3$ Gyr. Since the Phocaea asteroid family, which is the parent family of (5247) Krylov, is an old asteroid family whose age is 2.2 Gyr (Carruba 2009), we could imagine that (5247) Krylov might have experienced ∼1.7 times small or large collisions after its creation. Thus, it seems impossible that the Phocaea asteroid family has maintained its spin state since the period of its formation. We also need to consider the damping timescale, which is the time required for a NPA rotator to develop into a PA spin state. The PA spin state is the outcome of energy dissipation caused by stress-strain cycling. It is shown as $\tau_{\rm damping} = P_{obs}^3/C^3D_m^2$ where $C \simeq 36$ and P_{obs} is the rotational period expressed in hours (Pravec et al. 2014). P_{obs} will be determined and presented in a follow-up paper. We now take into account the damping timescale in four different cases, $P_{obs} = P_1 = 82.188$ h, $P_{obs} = P_2 = 67.37$ h, $P_{obs} = P_1/2 = 41.094$ h, and $P_{obs} = P_2/2 = 33.69$ h. These cases are based on the period analysis of the simulated light curve of a NPA rotator (Kaasalainen 2001); it is found to be $D_m = 10.44 \pm 0.37$ km using the same diameter and the collisional lifetime ($\tau_{\rm damping} \simeq 109$, 60, 4, and 8 Myr). It is impossible, however, that Krylov has maintained NPA rotation since the timescales in the above-mentioned cases are much smaller than its age (2.2 Gyr; Caruba 2009). As it orbits at a considerable distance from the major planets, no change in the spin state is expected caused by planetary flybys. Thus, (5247) Krylov is presumed to have experienced changes in its spin state due to either sub-catastrophic impact or YORP after its formation.

In addition, we may surmise that (5247) Krylov might have experienced sub-catastrophic impact after the Phocaea asteroid family was formed as Gil-Hutton (2006) predicted the presence of the Krylov group. However, there is still controversy about the presence of the Krylov group so it is too early to conclude that a sub-catastrophic impact was the immediate cause of its NPA rotation. Therefore, additional observations for the candidate members of the hypothetical Krylov group followed by physical modeling of this asteroid and suspected group members should be made. At the same time, studies on the possible influence of the YORP effect are required in order to establish the direct cause of its unstable spin state.

ACKNOWLEDGMENTS

This research is supported by the Korea Astronomy and Space Science Institute (KASI) and made use of the KMTNet system operated by KASI. Data were obtained at three host sites: CTIO in Chile, SAAO in South Africa, and SSO in Australia. The work of J.D. was supported by grant 15-04816S of the Czech Science Foundation.

REFERENCES

Bertin, E. 2005, Automatic Astrometric and Photometric Calibration with SCAMP, ASPC, 351, 112

Bowell, E., Hapke, B., & Domingue, D., et al. 1989, Application of Photometric Models to Asteroids, in Binzel, R. P., Gehrels, T., & Matthews, M. S., Asteroids II (Tucson: Univ. Arizona Press), 524

Buchheim, R. K. 2010, Methods and Lessons Learned Determining the H-G Parameters of Asteroid Phase Curves, SASS, 29, 101

Carruba, V. 2009, An Analysis of the Region of the Phocaea Dynamical Family, MNRAS, 398, 1512

Dandy, C. L., Fitzsimmons, A., & Collander-Brown, S. J. 2003, Optical Colors of 56 Near-Earth Objects: Trends with Size and Orbit, Icarus, 163, 363

Farinella, P., Vokrouhlicky, D., & Hartmann, W. K. 1998, Meteorite Delivery via Yarkovsky Orbital Drift, Icarus, 132, 378

Gil-Hutton, R. 2006, Identification of Families among Highly Inclined Asteroids, Icarus, 183, 93

Gilliland, R. L., & Brown, T. M. 1988, Time-Resolves CCD Photometry of an Ensemble of Star, PASP, 100, 754

Harris, A. W. 1994, Tumbling Asteroids, Icarus, 107, 209

Hudson, R. S., & Ostro, S. J. 1995, Shape and Non-Principal Axis Spin State of Asteroid 4179 Toutatis, Science, 270, 84

Jordi, K., Grebel, E. K., & Ammon, K. 2006, Empirical Color Transformations between SDSS Photometry and other Photometric Systems, A&A, 460, 339

Kaasalainen, M. 2001, Interpretation of Lightcurves of Precessing Asteroids, A&A, 376, 302

Karachkina, L. G. 1982, The Minor Planet Circulars/Minor Planets and Comets, MPC, 8723

Kim, M.-J. 2014, PhD thesis, Yonsei University, Korea

Kim, S.-L., Park, B.-G., & Chun, M.-Y. 1999, Variable Stars in the Open Cluster Mel 71, A&A, 348, 795

Kim, S.-L., Lee, C.-U., & Park, B.-G., et al. 2016, KMTNET: A Network of 1.6 M Wide-Field Optical Telescopes Installed at Three Southern Observatories, JKAS, 49, 37

Lenz, P., & Breger, M. 2005, Period04 User Guide, CoAst, 146, 53

Marsden, B. G., & Williams, G. V. 1993, The Minor Planet Circulars/Minor Planets and Comets, MPC, 22507

Moon, H.-K, Kim, M.-J., & Yim, H.-S., et al. 2015. International Astronomical Union Symposium, 318, 206

Munari, U., Henden, A., & Frigo, A., et al. 2014, APASS Landolt-Sloan BVgri Photometry of Rave Stars. I. DATA, Effective Temperatures, and Reddenings, AJ, 148, 81

Pravec, P., Harris, A. W., & Scheirich, P., et al. 2005. Tumbling Asteroids, Icarus, 173, 108

Pravec, P., Scheirich, P., & Ďurech, J., et al. 2014, The Tumbling Spin State of (99942) Apophis, Icarus, 233, 48

Scheirich, P., Ďurech, J., & Pravec, P., et al. 2010. The Shape and Rotation of Asteroid 2008 TC3, M&PS, 45, 1804

Sperl, M. 1998, Manual for Period98: V1.0.4; A Period Search-Program for Windows and Unix, CoAst, 111, 1

Usui, F., Kuroda, D., & Müller, T. G., et al. 2011, AcuA: the AKARI/IRC Mid-infrared Asteroid Survey, PASJ, 63, 1117

Vereš, P., Jedicke, R., & Fitzsimmons, A., et al. 2015, Absolute Magnitudes and Slope Parameters for 250,000 Asteroids Observed by Pan-STARRS PS1 – Preliminary Results, Icarus, 261, 34

Warner, B. D., Harris, A. W., & Pravec, P. 2009, The Asteroid Lightcurve Database, Icarus, 202, 134